Supplement of The Cryosphere, 19, 3329–3353, 2025
https://doi.org/10.5194/tc-19-3329-2025-supplement

The Cryosphere
Open Access

Supplement of

Loss of accumulation zone exposes dark ice and drives increased ablation at Weißseespitze, Austria

Lea Hartl et al.

Correspondence to: Lea Hartl (lea.hartl@oeaw.ac.at)

Section S1 SR50 data cleaning

The data records from the ultrasonic ranger (SR50) contain considerable noise. The exact cause of this problem has not been determined but is likely related either to a problem with the unheated sensor (the problem persisted to a lesser degree after the sensor was replaced), to spurious signals from a guy wire, the control box, rime or blowing snow, or a combination of these factors.

We used the SR50 data to determine surface height change throughout the 2018-2024 time series (Fig. S1) and estimate snowfall for the August 2021 period used for model evaluation (Fig. S2). A corresponding comparison of observed and modeled surface height is shown in Fig. S6.

SR50 data were smoothed as follows:

- Manual removal of outlier values with unrealistic amount of surface change or unrealistic surface values
- Removal of surface values where the difference between the value and the 48 hour rolling mean is greater than 15 cm.
- Extraction of the lower envelope of the remaining data and linear interpolation to fill resulting gaps.
- Computation of the 24 h rolling mean to smooth the resulting surface height time series
- Snowfall was calculated as the difference between consecutive hourly surface height values if the change is positive and set to zero if it is negative.

Fig. S3 shows an overview of data availability for the AWS dataset and additional data used in this study.

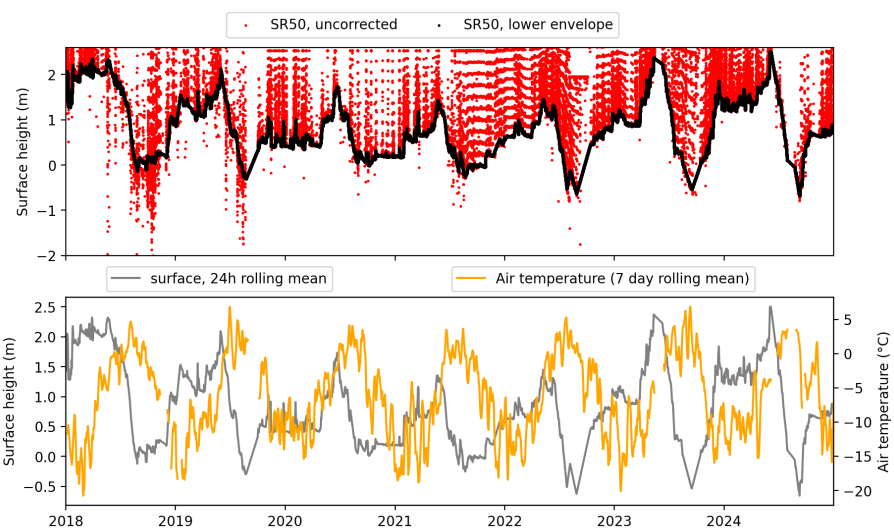

Figure S1. Upper panel: SR50 records without correction (red) and after smoothing and extraction of the lower envelope (black) for 2018 to 2024. Values are shown in relation to the height of the sensor above the ice surface at the time of installation (surface height = 0). Negative values indicate ice ablation since the time of installation. Lower panel: 24h rolling mean of surface height and 7 day rolling mean of air temperature.

Section S2 Impact of surface slope on daily albedo calculation

The glacier surface at the WSS AWS is slightly sloped in a northeasterly direction, at an angle of around 6°-8° degrees as per the 2017 DEM. The exact slope angle varies with snow cover and ice ablation and is unknown. The sensor alignment on the

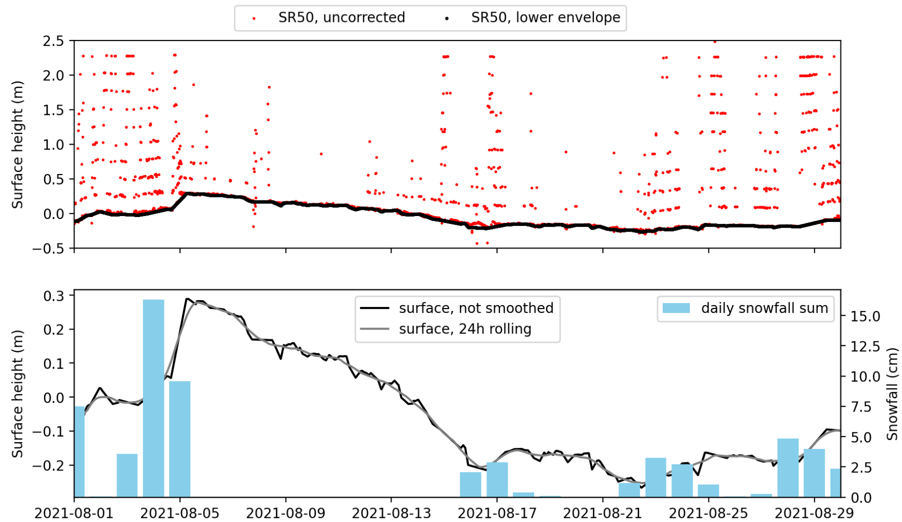

Figure S2. Upper panel: Same as previous figure, zoomed in on July 2021. Lower panel: Surface height as 24h rolling mean and daily snow fall sums.

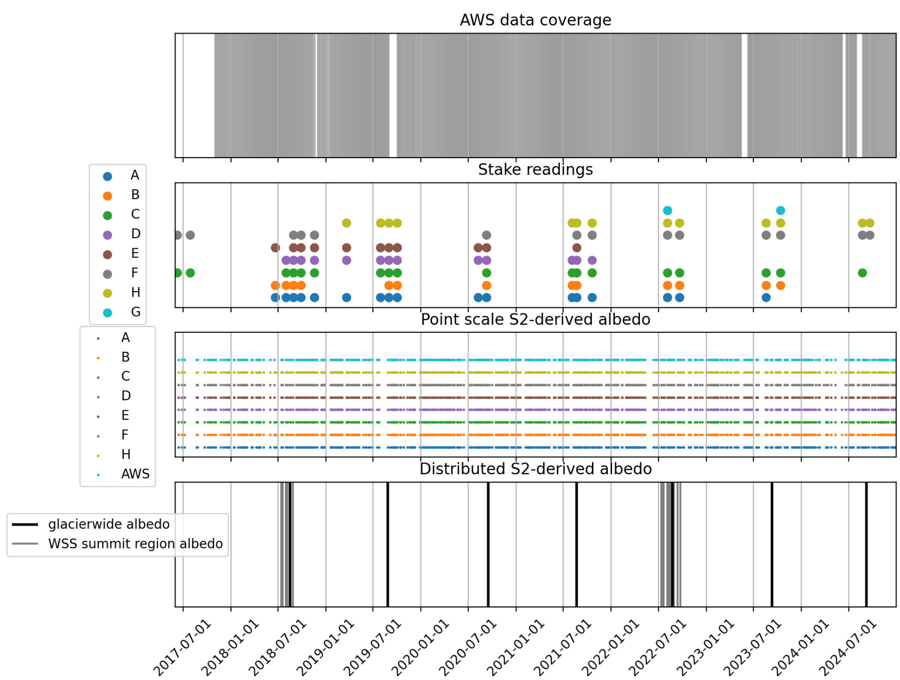

Figure S3. Overview of period of record and data availability of the different data types used in this study.

mast can deviate from the horizontal, especially in winter when the snow pack causes tension on the guy wires. The slope of the incident plane results in a systematic error in the measurement of reflected radiation (SW_{out}). On cloud free days, this

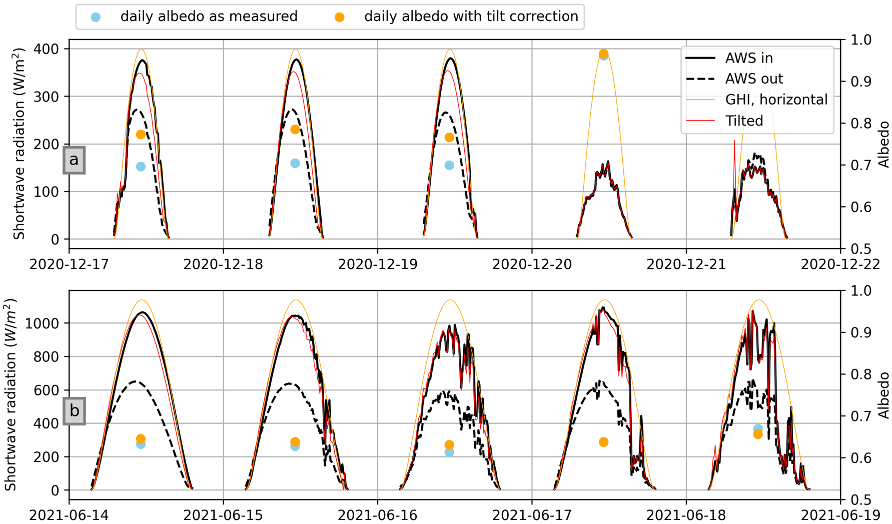

Figure S4. Diurnal cycle of incoming and reflected radiation for example time periods in winter (a) and summer (b). Black lines mark the measured shortwave incoming (AWS in) and reflected radiation (AWS out, dashed). Global hemispherical irradiance (GHI) for a horizontal surface was computed based on the sun angle and location. The red line indicates the irradiance for a plane with a slope angle of 6° and an aspect of 73° computed from the measured incoming radiation. Daily albedo as measured (SW_{ref}/SW_{in}) is shown in blue, the corrected albedo estimate in orange (SW_{ref}/SW_{tilted}).

is apparent in a temporal shift between the diurnal curves of incoming and reflected SW radiation such that the maximum of reflected SW radiation occurs before the maximum of incoming SW radiation (Fig. S4).

To estimate the magnitude of the potential impact of this effect on daily albedo, we corrected albedo based on the theoretical relationship between irradiance for horizontal and tilted planes of incidence, assuming a constant slope angle of 6° and an aspect of 73° (northeast). For a horizontal incident plane, albedo can be calculated as the ratio of reflected to incoming radiation:

$$albedo = \frac{SW_{out}}{SW_{in}}$$

In the case of a tilted reflecting surface, the measured parameter SW_{out} represents the incoming radiation on the tilted plane as reflected into the downward facing sensor, such that:

$$SW_{out} = SW_{tilted} * albedo$$

Where SW_{tilted} is a function of - mainly - SW_{in}, the solar position on a given day, and the slope and aspect of the surface. To assess the magnitude of the error introduced by the tilt of the surface, we computed a corrected albedo (albedo_cor) as the ratio of SW_{out} to SW_{tilted}. In addition to the solar position, calculating SW_{tilted} requires estimates of the diffuse horizontal irradiance (DHI) and direct normal irradiance (DNI) components of global hemispherical irradiance (GHI) as measured by the upward facing sensor. We applied Boland's method (Boland et al., 2013) as implemented in the python package pvlib (Anderson et al., 2023; Jensen et al., 2023) to decompose measured GHI (SW_{in}) into DNI and DHI. SW_{tilted} was then computed as the sum of direct beam irradiance and diffuse irradiance from the sky, both over the tilted plane of incidence, assuming an isotropic sky model also as implemented in the pvlib package.

The difference between raw and corrected values has a seasonal cycle determined by the sun angle and reaches highest values on cloud free days in the winter months. In summer, corrections are typically below +0.02 on cloud free days. On days with cloud cover, the correction values are negligible due to the increased contribution of diffuse radiation. For the entire data set, the median correction value is 0.04 in January, and 0.001 and 0.002 in July and August, respectively (Fig. S5). Hence, we consider the impact small compared to the assumed measurement uncertainty of the sensor. We note that other kinds of analyses may require more sophisticated corrections for the tilt, especially if addressing sub-daily resolution albedo during the winter months (Abermann et al., 2014; Weiser et al., 2016).

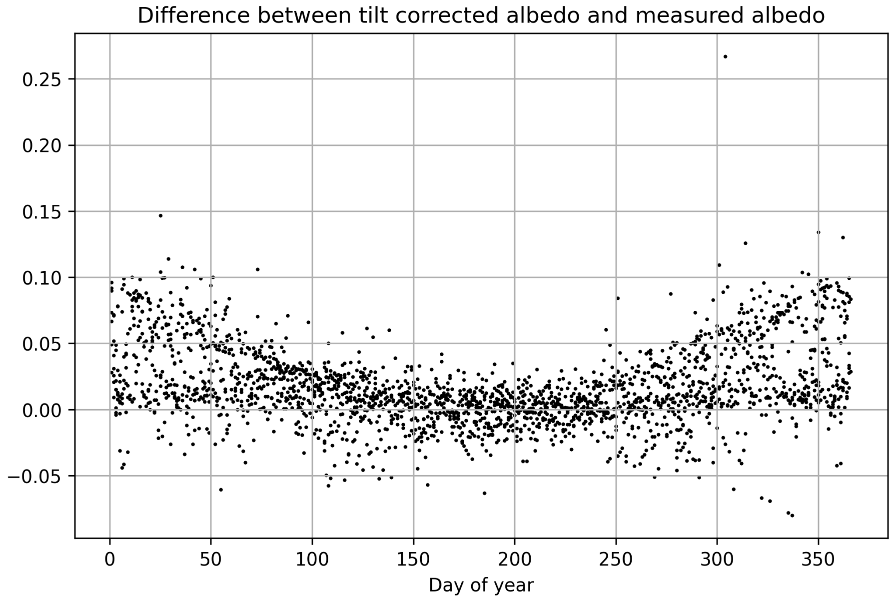

Figure S5. Difference between the daily albedo estimate corrected for the tilt of the surface and the uncorrected values plotted against the day of the year. Values are shown for the entire data set.

Section S3 Model evaluation

For the model evaluation (Fig. S6), an initial snow height of 28 cm was provided to the model. Initial snow density at the top and bottom of the snow pack was estimated as 200 and 350 kg m^{-3}, respectively. New snow density is kept constant at 68 kg m^{-3}. Model code as well as constants and further settings are provided in the following code repositories:

- Modified version used in this study: https://github.com/baldoa/cosipy_MSc/
- Main COSIPY repository: https://github.com/cryotools/cosipy
- The code to produce the figures and tables in this paper is available at: https://github.com/LeaHartl/WSS_Albedo

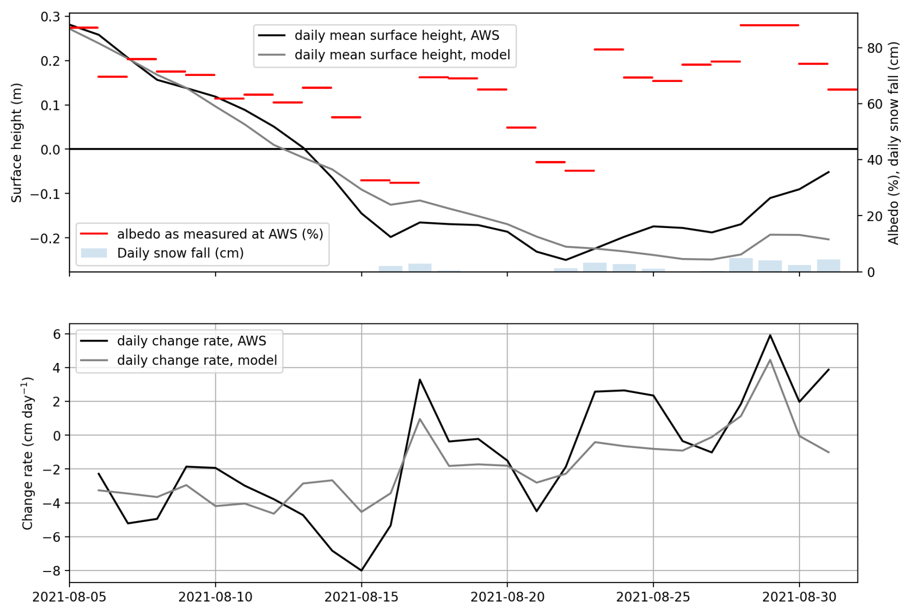

Figure S6. Upper panel: Daily mean surface height at the AWS in July 2021 as measured with the SR50 (smoothed as described above) and as COSIPY model output; daily albedo and snowfall (right axis) were used as input parameters for the model. Surface height is shown in reference to the ice surface at the time of installation of the SR50. Lower panel: Observed and modeled daily change rates.

Section S4 Additional supplementary material

Figure S7. Automatic camera images taken on or close to the date of the seasonal minimum albedo recorded by the AWS. Red ellipses indicate the AWS position. Photos were taken on August 21, 2018; August 24, 2019; September 20, 2020; August 15, 2021; August 11, 2022; August 25, 2023; September 8, 2024.

Figure S8. Photos of stakes A, C, and D and the AWS taken during stake readings on August 29, 2018.

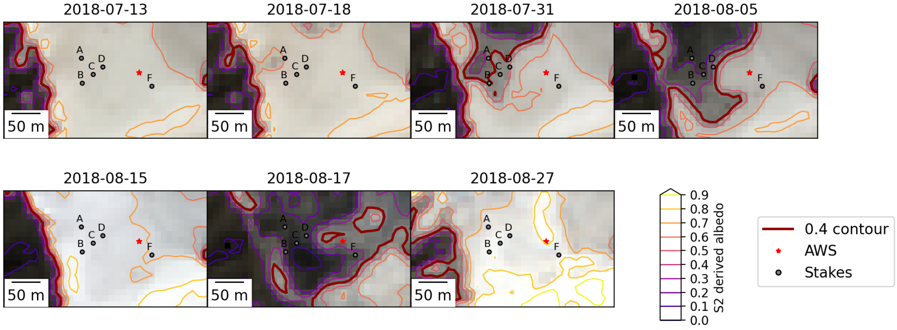

Figure S9. RGB composites of the WSS summit region in summer 2018. The contour lines indicate S2-derived albedo. The 0.4 contour ("low albedo" threshold) is highlighted as a thicker line.

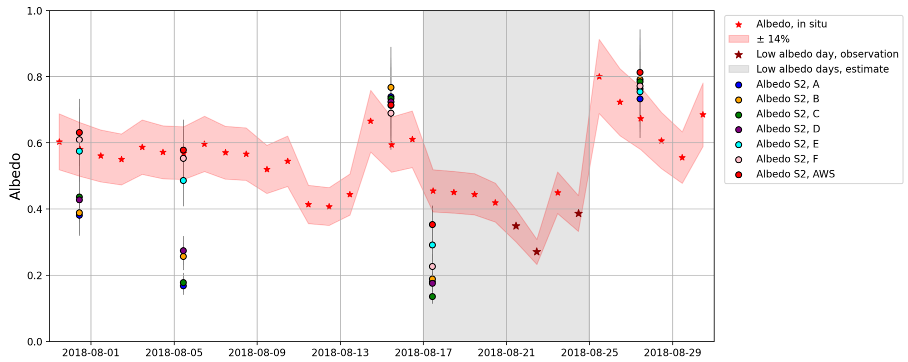

Figure S10. Daily albedo as observed at the AWS with ±14% uncertainty shown as red shading. S2-derived albedo at the stake locations and AWS shown as circular markers. Thin black lines indicate the estimated uncertainty of ±16% in the S2-derived albedo. The grey shading indicates the days counted as "estimated low albedo days" at the AWS.

Table S1. Modelled daily SMB averaged over 15 day time periods of average July-September conditions and different albedo values.

	SMB for albedo 0.10 [mm w.e.]	SMB for albedo 0.20 [mm w.e.]	SMB for albedo 0.40 [mm w.e.]	SMB for albedo 0.60 [mm w.e.]
Jul 1-Jul 15	-44	-39	-28	-17
Jul 16-Jul 30	-43	-38	-29	-19
Jul 31-Aug 14	-40	-36	-26	-17
Aug 15-Aug 29	-36	-32	-23	-15
Aug 30-Sep 13	-30	-26	-18	-11
Sep 14-Sep 29	-19	-15	-9	-4

References

Abermann, J., Kinnard, C., and MacDonell, S.: Albedo variations and the impact of clouds on glaciers in the Chilean semi-arid Andes, Journal of Glaciology, 60, 183–191, https://doi.org/https://doi.org/10.3189/2014JoG13J094, 2014.

Anderson, K. S., Hansen, C. W., Holmgren, W. F., Jensen, A. R., Mikofski, M. A., Driesse, A., et al.: pvlib python: 2023 project update, Journal of Open Source Software, 8, 5994, https://doi.org/https://doi.org/10.21105/joss.05994, 2023.

Boland, J., Huang, J., and Ridley, B.: Decomposing global solar radiation into its direct and diffuse components, Renewable and Sustainable Energy Reviews, 28, 749–756, https://doi.org/https://doi.org/10.1016/j.rser.2013.08.023, 2013.

Jensen, A. R., Anderson, K. S., Holmgren, W. F., Mikofski, M. A., Hansen, C. W., Boeman, L. J., and Loonen, R.: pvlib iotools—Open-source Python functions for seamless access to solar irradiance data, Solar Energy, 266, 112 092, https://doi.org/https://doi.org/10.1016/j.solener.2023.112092, 2023.

Weiser, U., Olefs, M., Schöner, W., Weyss, G., and Hynek, B.: Correction of broadband snow albedo measurements affected by unknown slope and sensor tilts, The Cryosphere, 10, 775–790, https://doi.org/https://doi.org/10.5194/tc-10-775-2016, 2016.